

Solar-like and Mira-like oscillations of stars – A uniform excitation mechanism *

Da-Run Xiong¹ and Li-Cai Deng²

¹ Purple Mountain Observatory, Chinese Academy of Sciences, Nanjing 210008, China;
xiongdr@pmo.ac.cn

² Key Laboratory for Optical Astronomy, National Astronomical Observatories, Chinese Academy of Sciences, Beijing 100012, China; licai@bao.ac.cn

Received 2013 May 12; accepted 2013 June 18

Abstract Using a non-local and time-dependent theory of convection, we have calculated the linear non-adiabatic oscillations of the radial and low-degree F-p39 modes for evolutionary models from the main sequence to the asymptotic giant branch for stars with solar abundance ($X = 0.70$, $Z = 0.02$) in the mass range of 0.6–3.0 M_{\odot} . The results show that low luminosity cool stars tend to be solar-like oscillators, whose low-order modes are stable, but intermediate and high order p-modes are pulsationally unstable; their unstable modes have a wide range in frequency and small values for amplitude growth rates. For stars with increasing luminosity and therefore lower temperature, the unstable modes shift towards lower orders, the corresponding range of frequency decreases, and the amplitude growth rate increases. High luminosity red giant stars behave like typical Mira-like oscillators. The effects of the coupling between convection and oscillations on pulsational instability have been carefully analyzed in this work. Our research shows that convection does not simply act as a damping mechanism for oscillations, and the complex nature of the coupling between convection and oscillations makes turbulent convection sometimes behave as damping, and sometimes as excitation. Such a picture can not only naturally account for the red edge of the instability strip, but also the solar-like oscillations in low luminosity red stars and Mira-like ones in high luminosity red giants.

Key words: convection — stars: oscillations — stars: late-type — stars: evolution

1 INTRODUCTION

The great discovery of solar five-minute oscillations (Leighton et al. 1962) made it possible for the first time to directly study the internal structure and motion of the Sun through observations and analysis of oscillations on the solar surface. The big leap forward in helioseismology encouraged astronomers to apply the same method to other stars. With continuous efforts in past decades, solar-like oscillations were eventually discovered in solar-like and sub-giant stars near the main sequence (MS) (Brown et al. 1991; Bouchy & Carrier 2002; Guenther et al. 2005; Bedding & Kjeldsen 2007) and red giants (Barban et al. 2007; Frandsen et al. 2002; Buzasi et al. 2000; De Ridder et al. 2009).

* Supported by the National Natural Science Foundation of China.

NASA's Kepler mission, with an accuracy higher than all other similar ground or space based observing missions, has collected stellar oscillation data for thousands of MS stars and red giants, which have enabled great progress in the field of asteroseismology (Chaplin et al. 2011a,b; Huber et al. 2011; Hekker et al. 2011).

It is popularly accepted that the five-minute oscillations of the Sun are excited by the stochastic effect of turbulence (Goldreich & Keeley 1977a,b; Kumar et al. 1988; Goldreich & Kumar 1988; Kumar & Goldreich 1989; Goldreich et al. 1994; Belkacem et al. 2008). As a natural extension, solar-like oscillations of stars have also been considered to be due to the same stochastic excitation of turbulence (Samadi & Goupil 2001; Samadi et al. 2003; Samadi et al. 2008). However, when Dziembowski et al. (2001) attempted to understand the observations of a red giant, α UMa, they discovered that such a mechanism is unable to explain the observed frequency spectrum and the amplitude of α UMa. The observed frequency dependence of the amplitude does not agree with the one expected from stochastic excitation. This mechanism predicts an amplitude of the fundamental mode, which may correspond to one of the largest observed amplitude modes, about two orders of magnitude smaller than the amplitudes of modes with $n \geq 5$. These luminous red giants can better be interpreted as Mira-like oscillators, instead of solar-like ones. By using our non-local and time-dependent theory of convection (Xiong 1989; Xiong et al. 1997), we have calculated the linear non-adiabatic oscillations of the Sun and red giants. Our results showed that all the g-modes and low-frequency F- and p-modes are pulsationally stable, but the intermediate- and high-frequency modes (with periods of $\approx 3 - 16$ min) are all unstable for the Sun (Xiong & Deng 2010). For luminous red giants, oscillation happens in the fundamental, low-order modes, and all the high-order modes are stable (Xiong et al. 1998a). The unstable mode shifts to higher orders with decreasing stellar luminosity (Xiong & Deng 2007). The successful interpretations of the oscillations of the Sun and red giants suggest that there is no distinct difference between solar-like and Mira-like oscillations in stars; both are naturally due to the interactions between convection and oscillations. This work aims to verify such a conjecture by detailed numerical modeling and analysis. A short description of our stellar convection theory, and the treatment of convection in our studies are given in Section 2. The results of our calculations are presented in Section 3. Section 4 is a thorough discussion of the excitation mechanism for low temperature stars. Conclusions of this work and discussions are presented at the end.

2 THEORETICAL TREATMENT OF CONVECTION

In a conventional HR diagram, the Cepheid instability strip crosses the plot from the upper-right to the lower-left, and includes all well-known classical pulsating variable stars, such as population I and II Cepheids, RR Lyrae, δ Scuti and pulsating white dwarfs. All of these classical pulsators are due to the radiative κ -mechanism. For the low-temperature stars located to the right of the strip, the ionization zones of hydrogen and helium that powers the κ -mechanism have already become fully convective. Obviously, convection overtakes radiation and becomes the major excitation and damping mechanism for oscillations. In a fluid medium with huge dimensions, such as in stellar interiors, convection usually becomes fully developed turbulence, whose properties and laws are not yet well understood. Therefore, it is not currently possible to have a complete theory describing convection. The pulsational stability of low-temperature stars having extended convective envelopes, such as the Sun and red giants, sensitively depends on the treatment of convection (Ulrich & Rhodes 1977; Antia et al. 1982; Antia et al. 1988; Gabriel 1988; Samadi et al. 2002; Dupret et al. 2006; Houdek 2008; Balmforth 1992). The most popularly applied theory of convection in calculations of stellar structure, evolution and oscillations is still the mixing-length theory (MLT, Böhm-Vitense 1958) and its various revisions, such as time-dependent MLT (Unno 1967; Gough 1977; Stellingwerf 1982; Grigahcène et al. 2005) and non-local MLT (Spiegel 1963; Ulrich 1970a,b).

For the study of stellar structure, MLT is still a very useful approximation. The reason is that convective energy transport is very efficient in deep stellar interiors. The temperature gradient in such conditions is very close to being adiabatic and is independent of the convection theory used. The depth of the outer convective zone of a star only depends on the structure of the so called super-adiabatic convection zone at the top, and is adjustable by tuning the mixing-length parameter.

The most obvious advantage of MLT is that it has a straightforward physical picture, and is very simple to apply. This is why MLT is widely used in current stellar modeling even though it still has quite an obvious problem. In fact, MLT does not follow from the hydrodynamic equations and turbulence theory, but is instead a phenomenological treatment. The fundamental shortcoming of MLT is that it cannot provide an accurate description for the dynamic behavior of turbulent convection. When dealing with dynamical problems of turbulent convection, such as time-dependent and non-local convection, this shortcoming becomes prominent. Considering such issues, a time-dependent and non-local theory of convection was then developed based on the hydrodynamic equations and theory of turbulence (Xiong 1981, 1989; Xiong et al. 1997). Compared with MLT, our theory has a more solid foundation in hydrodynamics, therefore it can provide a more precise treatment for the dynamics of turbulence. The simple physical picture in MLT is absent from our theory. In addition, it becomes more complicated than MLT in applications. The original MLT is described by a set of algebraic equations, but our time-dependent and non-local theory of convection is composed of three (for chemically uniform media) or six (for chemically non-uniform media) partial differential equations, each of which is second order in space. As a result, the equations of stellar envelope structure cover 10 orders, compared to four orders for the local MLT. For stellar evolution, at least 17 independent variables are needed (the exact number depends on the number of chemicals participating). Due to intrinsic singularities and stiff properties of the equations, numerical calculation becomes slightly difficult. That is the reason why such a theory cannot be generalized and widely applied in the community, and it is only used in a relatively small community of authors and their collaborators. Nevertheless, this community has enjoyed the successful application of such a theory to a number of studies in stellar problems, such as the structure of the solar convective zone (Unno et al. 1985), the depletion of lithium in the atmospheres of the Sun and solar-type stars (Xiong & Deng 2009), the structure and evolution of massive stars (Xiong 1985; Xiong 1986) and both radial and non-radial oscillations of stars (Xiong et al. 1998a, b; Xiong & Deng 2001a; Xiong & Deng 2007; Xiong & Deng 2010). Our studies have reproduced generally observed characteristics. For instance, reproducing the adiabatic sound speed inside the Sun from inversion of helioseismic data by using our non-local convection model as the reference model turns out to be much better than that from the standard solar model. (Zhang et al. 2012). It also reproduces the observation of lithium abundance in the atmospheres of the Sun and solar-like stars (Xiong & Deng 2009). Moreover, our theory not only offers a correct explanation for the red edge of the instability strip for RR Lyr (Xiong et al. 1998a,b) and δ Scu stars (Xiong & Deng 2001b), but also predicts the instability strip for Mira variables outside the Cepheid instability strip (Xiong & Deng 2007). The same theory also explains the observations and primary properties of small amplitude red variables (Xiong & Deng 2007).

The goal of the current work is to study the stability of radial and non-radial p-mode oscillations for solar-like stars and red giants. The energy generating core of a star has very little effect on p-mode oscillations, therefore our survey of pulsational stability for stars can be simplified to calculate the linear non-adiabatic oscillations of stellar envelope models. The structure and oscillations of stellar envelopes can be described by a set of seven equations, four of which are used to treat the conservations of mass, momentum and energy, and radiation transfer processes, therefore they are not very different from the traditional equations describing stellar structure. The only exceptions are that a Reynold tensor term of turbulence appears in the equation of momentum conservation, and turbulent thermal flux and turbulent kinetic energy terms are included in the equation of energy conservation. The other three equations describe the auto- and cross-correlations of turbulent velocity and temperature fluctuations, with all being second order partial differential equations. After a

simplification is applied to the third order correlations, these seven equations are then transformed to a consistent and closed set of dynamic equations for stellar structure and oscillations (Xiong 1989; Xiong et al. 1997). The linear stability analysis for these evolutionary models is divided into two steps:

- (1) Calculations of the non-local convective envelope models for stars:

If we set all the terms containing time derivatives and speed to be zero, we can derive the equations for calculating the model of a static envelope from our original ones. The complete set of equations and corresponding boundary conditions can be referred to in our previous work (Unno et al. 1985; Xiong & Deng 2001b).

- (2) Calculations of linear non-adiabatic oscillations using the envelope models:

Setting all variable quantities $y(r_0, t)$ be the sum of their equilibrium value and oscillation components, $y_0(r_0) + y'(r_0)e^{i\omega t}$, and taking a linear expansion around the equilibrium position, we can have a set of linear equations that describe non-adiabatic oscillations. For stellar radial oscillations, the equations have 10 dimensions; but for non-radial oscillations, there are 14 dimensions. The equations representing linear oscillations and boundary conditions can be found in our previous work (Xiong et al. 1998a; Xiong & Deng 2007). For non-radial oscillations, a concise description can be found in a recent paper (Xiong & Deng 2010).

Being different from the usual theoretical scheme of stellar oscillations, the completely non-local treatment of convection is used either in equilibrium models or pulsation calculations. This is a key point because, for low temperature stars having extended convective envelopes, the dynamical coupling between convection and oscillations is as important as the thermodynamic coupling, and is sometimes more important. Non-local convection is vitally significant for the stability of low temperature stars. This is why the results of our theoretical calculations are so different from those that use normal MLT.

3 THE NUMERICAL RESULTS

With the algorithm discussed in the previous section, we calculated the radial and low-degree ($l = 1 - 4$) non-radial, non-adiabatic oscillations for stars from the MS up to the red giant and asymptotic giant branch (AGB) phases in the mass range $0.6 - 3.0 M_{\odot}$. The upper boundary is placed at the optical depth of $\tau = 10^{-3}$, and the lower boundary at an arbitrarily deep enough radius: $T_b \approx 8 \times 10^6$ K for MS, sub-giant and low luminosity red giant stars, or $r_b/R_0 \approx 0.01$ for more luminous red giants, where T_b and r_b are respectively the temperature and radius of the bottom boundary. The equation of state (Hummer & Mihalas 1988; Daeppen et al. 1988) and OPAL opacity (Rogers & Iglesias 1992) have been used in this work. For the low temperature regime, the opacity has been supplemented with the low temperature table of Alexander & Ferguson (1994). Linear non-adiabatic oscillations of the fundamental up to the 39th p-mode are modeled.

3.1 Pulsationally Stable and Unstable Modes in the H-R Diagram

Figure 1(a) and (b) shows respectively the distributions of stable (small solid dots) and unstable (open symbols and crosses) radial modes in the H-R diagram. It is clearly shown from Figure 1(a) that the unstable modes with a lower degree form two well-separated groups, i.e. the one for well-known δ Scuti stars located in the central part of the diagram, and another one on the upper right part for pulsating red giants, including Miras, semi-regular and irregular variables. As demonstrated in Figure 1(a) and (b), all the low luminosity stars located to the right of the δ Scuti instability strip are stable in lower order modes, but are unstable in intermediate- and high-order modes. These stars have solar-like oscillatory properties. On the contrary, all the high luminosity red giants are unstable in low-degree modes, while at the same time being stable in intermediate- and high-order modes.

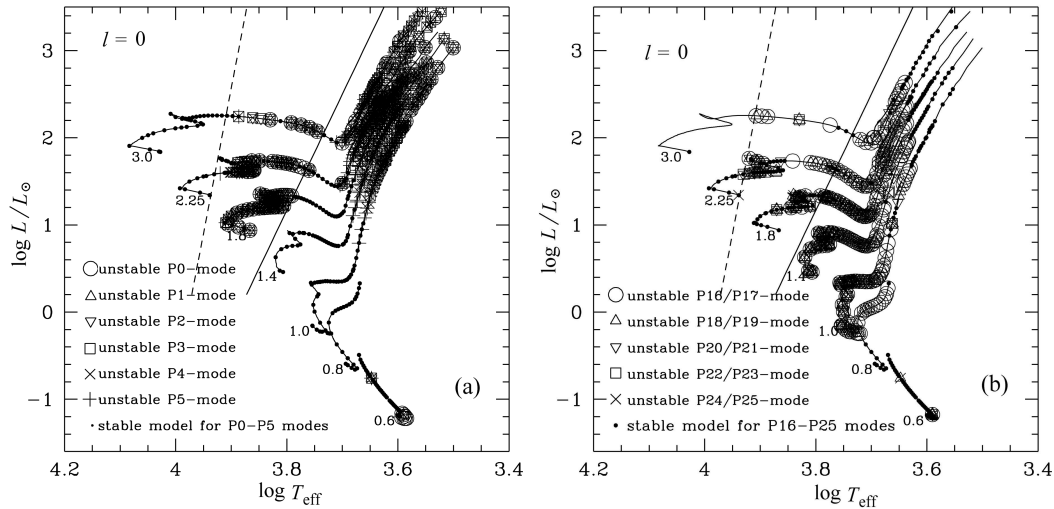


Fig. 1 Pulsationally stable (*small dots*) and unstable (*open symbols and crosses*) radial modes on the H-R diagram. Panel (a): the low-order (p0–p5) modes. Panel (b): the intermediate- and high-order (p16–p25) modes. The dashed- and solid-lines are, respectively, the theoretical blue and red edges of the δ Scuti instability strip.

They are typical Mira-like oscillators. On Figure 1(b), the solar-like instability strip has already been connected with the δ Scuti strip. In fact, these two classes of variable stars have distinctly different characters.

The δ Scuti stars are mainly excited by the radiation κ -mechanism, and the solar-like oscillators in the right hand side of the δ Scuti instability strip are excited by convection. The δ Scuti stars oscillate in intermediate- and low-order modes, but the solar-like stars with low-temperatures and about the same luminosities are oscillating in intermediate- and high-order modes. We are going to show that the normalized frequency (or radial order) of the maximum unstable mode for solar-like oscillations depends primarily on stellar luminosity and weakly on temperature. For example, for a low temperature star located outside the instability strip, with $M = 2 M_{\odot}$, $\log(L/L_{\odot}) \approx 1.45$ and $\log T_e \approx 3.69$, its maximum unstable mode is p15. However, for a δ Scuti star with similar luminosity, its maximum unstable mode is p4.

3.2 Pulsationally Stable and Unstable Modes in the $\log L/L_{\odot} - n_r$ Plane

A trend has been demonstrated in Figure 1(a) and (b): for increasing stellar luminosity, the oscillation instability tends to shift from high order modes to lower order ones.

Figure 2 shows the distribution of the stable (small solid dots) and unstable radial modes (open circles) in the $\log L/L_{\odot} - n_r$ plane for evolutionary models of an $M = 1.0 M_{\odot}$ star, where n_r is the radial order of the modes. The size of the circles in the plot is proportional to the logarithm of amplitude growth rate $\log \eta$, where $\eta = -2\pi\omega_i/\omega_r$, and ω_i and ω_r are respectively the imaginary and real parts of the complex circular frequency $\omega = \omega_r + \omega_i i$. As clearly shown in Figure 2, for increasing stellar luminosity, oscillations proceed from high-order modes towards lower order modes, and the number of unstable modes decreases, while the amplitude growth rates increase.

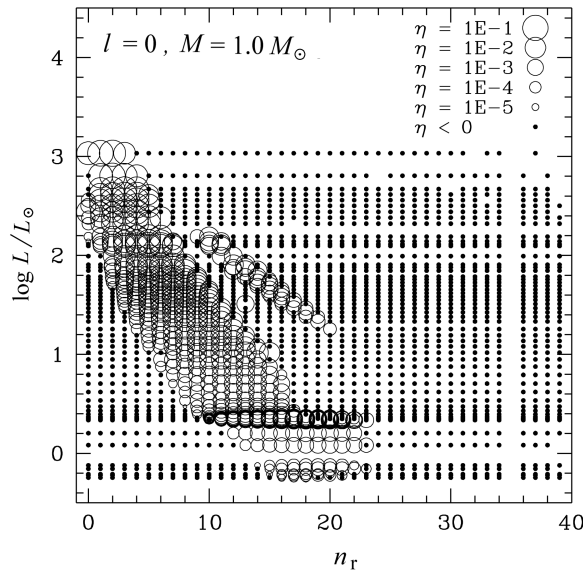


Fig. 2 Pulsationally stable (*small dots*) and unstable (*open circles*) radial modes on the $\log L/L_{\odot} - n_r$ plane for the evolutionary models of an $M = 1.0 M_{\odot}$ star, where n_r is the radial order of modes. The size of the circles is proportional to the logarithm of the amplitude growth rate of the oscillation modes.

3.3 The Dependence of Pulsation Amplitude Growth Rate on l and ν

The classical giant variables, such as Cepheids and RR Lyrae stars, are usually oscillating in the radial fundamental mode, or sometimes in a few low order overtones, with large amplitudes. The most obvious characteristics of the solar five-minute oscillations and solar-like oscillations of stars are simultaneous excitation of multiple modes, both radial and non-radial. The amplitudes are tiny. For the oscillations of the Sun, over 10^7 modes with l from 0 to ~ 1000 have been observed. Individual modes have amplitudes ranging from a few millimeters per second up to about 20 centimeters per second. Our studies show that the theoretical amplitude growth rates of the oscillations only depend on the oscillation frequencies ν , not on the degree l of the spherical harmonics; this is true at least for the intermediate- and low-degree modes of $l \leq 25$ (Xiong & Deng 2010). Through the current work, we have learned that the same fact also holds for the pure p-mode oscillations of stars other than the Sun.

Figure 3 shows the amplitude growth rates (η) of the non-radial modes with $l = 1 - 4$ as a function of frequency $\nu (= \omega_r/2\pi)$ for the solar model. Such a theoretical result has been confirmed by observations of solar oscillations (Libbrecht & Zirin 1986; Libbrecht 1988; Libbrecht & Woodard 1991).

3.4 The Maximum Unstable Mode

As shown in Figure 3, the amplitude growth rates for solar-like oscillations vary as a function of frequency of the oscillation mode. In this work, the maximum unstable mode is defined as the mode whose amplitude growth rate is the largest for a given stellar model. Because the oscillatory amplitude of any individual mode is always extremely small for solar-like oscillators, the non-linearity

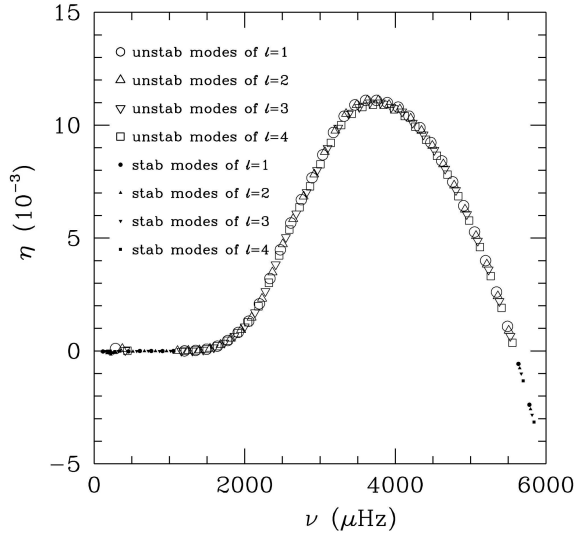


Fig. 3 The amplitude growth rates $\eta = -2\pi\omega_i/\omega_r$ versus frequencies for the Solar model.

has little effect on selection of modes. Therefore we expect that the theoretical prediction for the maximum unstable mode should correspond to the mode of maximum amplitude observed, when the coupling between convection and oscillations is treated in the right way.

Figures 1 and 2 show a trend: towards higher luminosity, the oscillation instability shifts from high- or intermediate-orders to lower ones, and the amplitude growth rate also increases at the same time.

Figures 4 and 5 demonstrate respectively the radial order n_{\max} and its amplitude growth rate η_{\max} of the maximum unstable mode as functions of luminosity for the low temperature stars of 1.0 to 3.0 M_{\odot} located to the right hand side of the instability strip. In Figure 4, the open symbols represent the radial modes, while the small solid symbols are the non-radial modes of $l = 1 - 4$. It can be seen that the radial orders of the maximum unstable mode decrease almost linearly with increasing $\log L/L_{\odot}$ for stars with the same mass. It is also shown in Figure 5 that the amplitude growth rate hardly depends on stellar mass and the spherical harmonic degree l ; instead it depends exclusively on luminosity. $\log \eta$ increases almost linearly with $\log L/L_{\odot}$.

Similar to the pulsation constant Q , we define the normalized oscillation frequency as the following,

$$[\nu] = \nu \sqrt{\frac{\bar{\rho}_{\odot}}{\bar{\rho}}}. \quad (1)$$

By using linear pulsation stability analysis, we found that the normalized frequency of the maximum unstable mode $[\nu]$ can be approximately expressed as,

$$\log [\nu_{\max}] \approx 1.5 \log \frac{T_e}{T_{e\odot}} - 6.5 \left[\log \frac{T_e}{T_{e\odot}} \right]^2 - 0.1 \log \frac{M}{M_{\odot}} + 3.47. \quad (2)$$

Figure 6 shows the term $\log [\nu_{\max}] + 0.1 M/M_{\odot}$ as a function of effective temperature, from which one can see that Equation (2) is validated for all the radial and non-radial modes for low-temperature stars of 0.6–3.0 M_{\odot} , located to the right hand side of the instability strip.

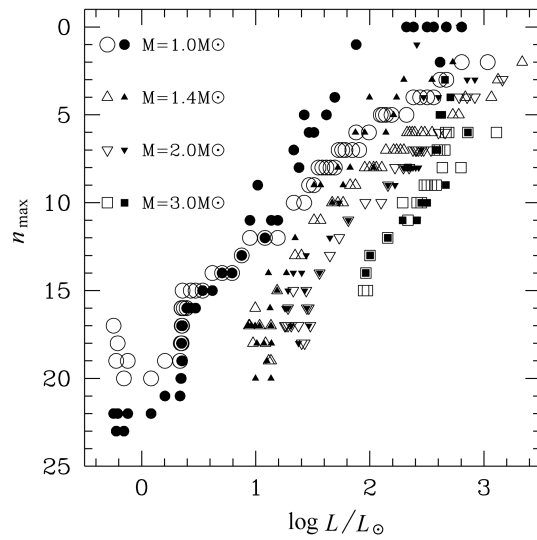


Fig. 4 The radial order of the maximum unstable mode versus stellar luminosity for evolutionary models of stars with $M = 1 - 3 M_{\odot}$. The open and solid symbols are, respectively, the radial and low-degree non-radial modes.

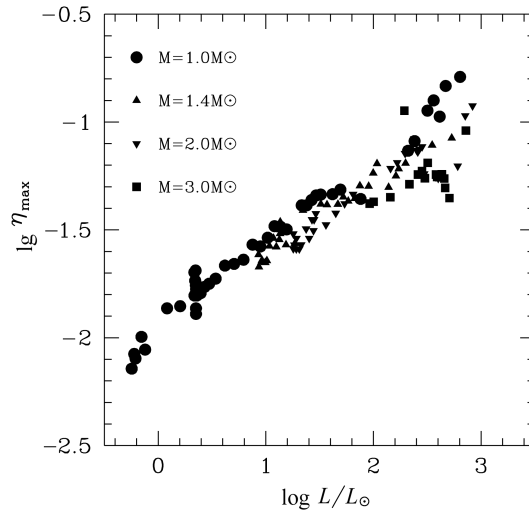


Fig. 5 The amplitude growth rate of the maximum unstable mode versus stellar luminosity for evolutionary models with $M = 1 - 3 M_{\odot}$.

Brown et al. (1991) argued that $\nu_{\max} \propto C_s/H_P$, where C_s is the sound speed and $H_P \propto T/g$ is the pressure scale height of the stellar atmosphere, and then calibrated such a rigid relation using a solar model and derived the following semi-empirical relation for the maximum unstable frequency,

$$\nu_{\max} = \frac{(M/M_{\odot})(T_e/5777)^{3.5}}{L/L_{\odot}} \nu_{\max\odot}, \quad (3)$$

where $\nu_{\max\odot} = 3021 \pm 27 \mu\text{Hz}$ is the frequency of the maximum unstable mode of the Sun.

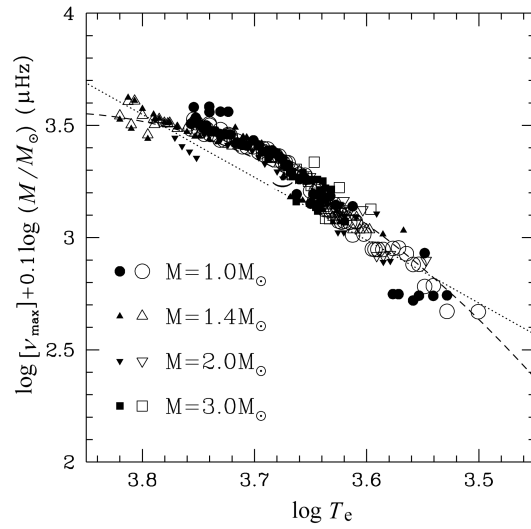


Fig. 6 The normalized frequencies of the maximum unstable modes versus the effective temperature for evolutionary models of stars with $M = 1 - 3 M_{\odot}$. The open and solid symbols are, respectively, the radial and low-degree non-radial modes.

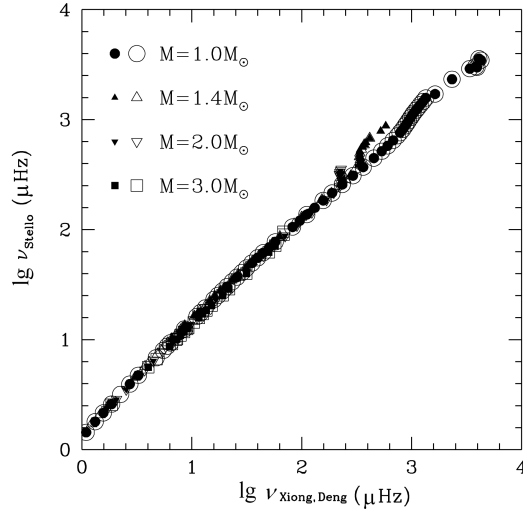


Fig. 7 A comparison between our theoretical results and the semi-empirical formula Eq. (3) (Stello et al. 2007).

From Equations (1) and (2), the frequency of the maximum unstable mode predicted by our theoretical calculations of non-adiabatic oscillations of stars can be transformed to,

$$\log \nu_{\max} = 4.5 \log \frac{T_e}{T_{e\odot}} - 6.5 \left[\log \frac{T_e}{T_{e\odot}} \right]^2 - 0.75 \log \frac{L}{L_{\odot}} + 0.4 \log \frac{M}{M_{e\odot}} + 3.47. \quad (4)$$

In Figure 7, a comparison is presented between the theoretically predicted (from Eq. (4)) frequency of the maximum unstable mode in our non-adiabatic oscillation theory to that of Stello et al.'s equation (3). A very good match has been reached, as demonstrated in the plot.

4 THE EXCITATION MECHANISM OF OSCILLATIONS FOR LOW-TEMPERATURE STARS ON THE RIGHT HAND SIDE OF THE INSTABILITY STRIP

It is well known that warm pulsating variable stars such as Cepheids, RR Lyrae and δ Scuti are excited by the radiative κ -mechanism. For cooler stars located to the right hand side of the instability strip, the major mechanism for energy transportation in the envelope is convection, instead of radiation. Naturally, convection should become the primary mechanism of excitation and damping for oscillations in these cool stars. For a long time, people have thought that the coupling between convection and oscillations is solely a damping against p-mode oscillations of stars, which results in the red edge of the instability strip. The oscillations in the Sun and all low-temperature stars located to the right hand side of the instability strip are damped out by convection, therefore these stars should be pulsationally stable (Balmforth 1992). Solar five-minute oscillations and the solar-like oscillations of stars are excited by stochastic excitation of turbulent convection (Goldreich & Keeley 1977a,b; Kumar et al. 1988; Goldreich & Kumar 1988; Kumar & Goldreich 1989; Goldreich et al. 1994; Belkacem et al. 2008; Samadi & Goupil 2001; Samadi et al. 2003; Samadi et al. 2008). Such an idea was supported by the finite line width of solar p-mode oscillations (Libbrecht 1988). However, this idea is rather superficial. Even if the turbulent stochastic excitation can explain the five-minute oscillations fairly well and also explain the solar-like oscillations in MS stars and sub-giant stars, there are great difficulties in applying the same mechanism to solar-like oscillations observed in intermediate- and high-luminosity red giants, such as α UMa (Dziembowski et al. 2001) discussed in Section 1. It is impossible to explain the huge pulsation amplitudes and the frequency spectra of unstable mode in Miras, semi-regular and irregular variable stars. Convection affects the stability of stars in three ways: turbulent thermal convection, turbulent pressure and turbulent viscosity. We will see below that turbulent viscosity and turbulent thermal convection play a damping effect against oscillations, however turbulent pressure is usually a destabilizing effect. The aspect ratios among the three factors actually change with the structure of stars (as functions of luminosity, effective temperature and metallicity) and the mode of oscillations. Sometimes convection overall behaves as a damping mechanism, and sometimes as an excitation. The key question for exploring the pulsational stability of low-temperature stars is that one needs a well established non-local and time-dependent theory of convection to handle the coupling between convection and oscillations.

4.1 Accumulated Work

In the above discussions, a qualitative picture of the coupling between convection and oscillations is presented. In the following, we are going to start from the hydrodynamic equations (the conservation equations of energy and momentum of mean motions), and dynamic equations for turbulent correlations, to derive the expressions for the accumulated work done by stellar oscillations, and to quantitatively describe the excitation and damping of oscillations due to the radiation and the coupling between convection and oscillations. Without loss of generality, all the mathematics of stellar convective motions follow Reynold's method. Due to the gigantic scale of stars, stellar convection occurs in fully developed turbulence, therefore all the physical quantities X will be expressed as the sum of its averaged value \overline{X} and its turbulent fluctuation X' ,

$$X = \overline{X} + X'. \quad (5)$$

Inserting Equation (5) into the dynamic equations for fluids, and expanding a Taylor series for X' and saving only the first order of X' , then averaging all the equations, we can have the hydrodynamic

equations for average motion. The equations describing conservation of energy and momentum, for instance, can be transformed into the following average equations of the corresponding conservation laws after Reynold's decomposition and the averaging process,

$$\frac{D\bar{u}^i}{Dt} + \frac{1}{\bar{\rho}} \nabla_k \left(g^{ik} \bar{P} + \overline{\rho u^i u^k} \right) + g^{ik} \nabla_k \bar{\phi} = 0, \quad (6)$$

$$\begin{aligned} & \bar{\rho} \bar{C}_P \frac{D\bar{T}}{Dt} - \bar{B} \frac{D\bar{P}}{Dt} + \frac{1}{2} \bar{\rho} \frac{D}{Dt} \overline{u_i^i u^i} + \overline{\rho u^i u^k} \nabla_k \bar{u}_i \\ & = \bar{\rho} \bar{\epsilon}_N - \nabla_k \left(\bar{F}_r^k + \bar{F}_c^k + \bar{F}_t^k \right), \end{aligned} \quad (7)$$

where $\bar{F}_r^k, \bar{F}_c^k = C_P \overline{\rho u^k T'}$ and $\bar{F}_t^k = \overline{\rho u^k u_i^i u^i}$ are respectively the radiative, convective and turbulent kinetic energy fluxes, and

$$\frac{D}{Dt} = \frac{\partial}{\partial t} + \bar{u}^k \nabla_k \quad (8)$$

is the Lagrangian differential operator, and ρ, T, P, ϵ_N and u^i are respectively the density, temperature, pressure, nuclear energy generation rate per unit mass and the i th covariant component of the velocity of the gas, ϕ is the gravitational potential, C_P is the specific heat at constant pressure, $B = -(\partial \ln \rho / \partial \ln T)_P$ is the expansion coefficient of gas and F_r^k is the k component of radiative flux.

It is shown in Equations (6) and (7) that, when convection happens, a turbulent Reynold's stress term $\overline{\rho u^i u^k}$ emerges in the equation describing momentum conservation in fluid motion, turbulent thermal flux F_c and turbulent kinetic energy flux F_t . The Reynold's stress can be expressed by the sum of the isotropic component $g^{ik} \bar{\rho} x^2$ and anisotropic component $\bar{\rho} \chi^{ik}$,

$$\overline{\rho u^i u^k} = \bar{\rho} (g^{ik} x^2 + \chi^{ik}). \quad (9)$$

By subtracting the average Equations (6) and (7) from the original conservation equations of momentum and energy, one can get the dynamic equations of turbulent velocity u^i and relative temperature fluctuation T'/\bar{T} , and then the dynamic equations for the auto- and cross-correlations of turbulent velocity and temperature fluctuation. The resulting equations, together with the equations for average motion of a fluid, form a complete, closed and consistent set of dynamic equations for stellar structure and oscillations (Xiong 1989; Xiong et al. 1997). The dynamic equations for the isotropic component x^2 and the anisotropic one of turbulent Reynold's stress can be expressed in the following (Deng et al. 2006):

$$\begin{aligned} & \frac{Dx^2}{Dt} + \frac{2}{3} (x^2 \nabla_k \bar{u}^k + \chi^{ik} \nabla_k \bar{u}_i) - \frac{2}{3} \overline{B u^k} \frac{T'}{\bar{T}} \left(\frac{D\bar{u}_k}{Dt} + \nabla_k \bar{\phi} \right) \\ & - \frac{1}{\bar{\rho}} g^{\alpha\beta} \nabla_\alpha (\bar{\rho} x^l \nabla_\beta x^2) = -\frac{4}{3\tau_c} x^2, \end{aligned} \quad (10)$$

$$\begin{aligned} & \frac{D\chi^{ij}}{Dt} + x^2 \left(g^{ik} \nabla_k \bar{u}^j + g^{jk} \nabla_k \bar{u}^i - \frac{2}{3} g^{ij} \nabla_k \bar{u}^k \right) \\ & + \chi^{ik} \nabla_k \bar{u}^j + \chi^{jk} \nabla_k \bar{u}^i - \frac{2}{3} g^{ij} \chi^{\alpha\beta} \nabla_\alpha \bar{u}_\beta \\ & - \bar{B} \left(g^{ik} \overline{u^j} \frac{T'}{\bar{T}} + g^{jk} \overline{u^i} \frac{T'}{\bar{T}} - \frac{2}{3} g^{ij} \overline{u^k} \frac{T'}{\bar{T}} \right) \left(\frac{D\bar{u}_k}{Dt} + \nabla_k \bar{\phi} \right) \\ & - \frac{1}{\bar{\rho}} g^{\alpha\beta} \nabla_\alpha (\bar{\rho} x^l \nabla_\beta \chi^{ij}) = -\frac{4(1+c_3)}{3\tau_c} \chi^{ij}, \end{aligned} \quad (11)$$

where

$$\tau_c = \frac{c_1 r^2 \bar{P}}{0.78 G M_r \bar{\rho} x} \quad (12)$$

is the decay timescale of turbulence due to viscosity, and

$$l = \frac{\sqrt{3}}{4} c_2 H_P = \frac{\sqrt{3} c_2 r^2 \bar{P}}{4 G M_r \bar{\rho}} \quad (13)$$

is the characteristic scale length of the turbulent diffusion. c_1 , c_2 and c_3 are the convection parameters related respectively to turbulent viscous dissipation, non-local diffusion and anisotropy of turbulence (Xiong 1989; Xiong et al. 1997; Deng et al. 2006).

The anisotropic component of Reynold's stress χ^{ij} is a symmetric ($\chi^{ij} = \chi^{ji}$) second order tensor, which contains, in general, six independent components. However, for static convection or radial oscillations in stars, only three components in the diagonal χ^{11} , χ^{22} and χ^{33} are non-zero due to spherical symmetry; all the other non-diagonal components are zero, i.e. $\chi^{12} = \chi^{23} = \chi^{31} = 0$. Moreover, as $g_{ij}\chi^{ij} = 0$, only one of the non-zero components is independent,

$$g_{11}\chi^{11} = \chi_1^1 = -2\chi_2^2 = -2\chi_3^3. \quad (14)$$

Using Equation (14), one can prove that, for stellar radial oscillations, Equation (6) can be simplified as,

$$\frac{D\bar{u}_r}{Dt} + 4\pi r^2 \frac{\partial}{\partial M_r} (\bar{P} + \bar{\rho}x^2) + \frac{4\pi}{r} \frac{\partial}{\partial M_r} (\bar{\rho}r^3\chi_1^1) + \frac{GM_r}{r^2} = 0, \quad (15)$$

and Equations (10) and (11) can be simplified to,

$$\begin{aligned} \frac{Dx^2}{Dt} + \frac{2}{3} \left[-\frac{x^2}{\bar{\rho}} \frac{D\bar{\rho}}{Dt} + \chi_1^1 \frac{\partial}{\partial \ln r} \left(\frac{\bar{u}_r}{r} \right) \right] \\ - \frac{2}{3} B u_r \frac{\overline{T'}}{\overline{T}} \left(\frac{D\bar{u}_r}{Dt} + \frac{GM_r}{r^2} \right) \\ - \frac{1}{\bar{\rho}r^2} \frac{\partial}{\partial r} \left(r^2 \bar{\rho} x l \frac{\partial x^2}{\partial r} \right) = -\frac{4}{3\tau_c} x^2, \end{aligned} \quad (16)$$

$$\begin{aligned} \frac{D\chi_1^1}{Dt} + \frac{4}{3} \left\{ x^2 \frac{\partial}{\partial \ln r} \left(\frac{\bar{u}_r}{r} \right) + \chi_1^1 \left[\frac{\partial}{\partial \ln r} \left(\frac{\bar{u}_r}{r} \right) + \frac{3}{2} \frac{\bar{u}_r}{r} \right] \right\} \\ - \frac{4}{3} B u_r \frac{\overline{T'}}{\overline{T}} \left(\frac{D\bar{u}_r}{Dt} + \frac{GM_r}{r^2} \right) - \frac{1}{\bar{\rho}r^2} \frac{\partial}{\partial r} \left(r^2 \bar{\rho} x l \frac{\partial \chi_1^1}{\partial r} \right) \\ = -\frac{4(1+c_3)}{3\tau_c} \chi_1^1. \end{aligned} \quad (17)$$

Now, linearizing Equation (15) gives,

$$\begin{aligned} \omega^2 \delta r = \frac{1}{\bar{\rho}} \frac{d}{dr} [\delta \bar{P} + \delta (\bar{\rho}x^2)] + \frac{1}{\bar{\rho}r^3} \frac{d}{dr} [\delta (\bar{\rho}r^3\chi_1^1)] \\ - \left[4 \frac{GM_r}{r^3} + \frac{3}{\bar{\rho}r^3} \frac{d(\bar{\rho}r^3\chi_1^1)}{dr} \right] \delta r. \end{aligned} \quad (18)$$

Multiplying Equation (18) by $\delta r^* dM_r$, and integrating from 0 to M_0 with respect to dM_r , the left hand side becomes,

$$\int_0^{M_0} \omega^2 \delta r \delta r^* dM_r = 2 \left(1 + \frac{\omega_i^2}{\omega_r^2} + 2i \frac{\omega_i}{\omega_r} \right) E_K, \quad (19)$$

where

$$E_K = \frac{1}{2}\omega_r^2 \int_0^{M_0} \delta r \delta r^* dM_r, \quad (20)$$

is the total kinetic energy of the corresponding mode, and ω_i and ω_r are respectively the imaginary and real parts of the complex circular frequency of the oscillatory mode $\omega = \omega_r + i\omega_i$. With simple manipulation, the accumulated work can be expressed as,

$$\begin{aligned} W_{\text{all}} &= -2\pi \frac{\omega_i}{\omega_r} \\ &= \frac{\pi}{2E_K} \int_0^{M_0} \text{Im} \left\{ - \left[\frac{\delta \bar{P}}{\bar{\rho}} + 2x^2 \frac{\delta x}{x} \right] \frac{\delta \bar{\rho}^*}{\bar{\rho}} + \delta \chi_1^1 \frac{d}{d \ln r} \left(\frac{\delta r^*}{r} \right) \right\} dM_r. \end{aligned} \quad (21)$$

4.2 Radiative κ -Mechanism and Radiative Modulation Excitation

Equation (21) is the proper expression for the accumulated work involved in stellar radial oscillations. The second and third terms in the integral represent contributions due to the isotropic (δx^2) and anisotropic ($\delta \chi_1^1$) components of the Reynold's stress, in other words, the dynamical coupling between convection and oscillations. The first term including δP is the gas pressure component in the accumulated work,

$$W_{P_g} = -\frac{\pi}{2E_K} \int_0^{M_0} \text{Im} \left[\frac{\delta \bar{P}}{\bar{\rho}} \frac{\delta \bar{\rho}^*}{\bar{\rho}} \right] dM_r. \quad (22)$$

Linearizing the equation of energy conservation given by Equation (7), for radial oscillations we have,

$$\begin{aligned} \frac{\delta \bar{P}}{\bar{P}} &= \Gamma_1 \frac{\delta \bar{\rho}}{\bar{\rho}} + \frac{\Gamma_3 - 1}{\bar{P}} \left\{ \bar{\rho} x^2 \left(\frac{\delta \bar{\rho}}{\bar{\rho}} - 3 \frac{\delta x}{x} \right) \right. \\ &\quad \left. - \bar{\rho} \chi_1^1 \frac{d}{d \ln r} \left(\frac{\delta r}{r} \right) \right. \\ &\quad \left. + \frac{1}{i\omega} \left[\delta (\bar{\rho} \epsilon_N) - \frac{1}{4\pi r^2} \frac{d}{dr} (\delta L_r + \delta L_c + \delta L_t) \right] \right\}. \end{aligned} \quad (23)$$

The first term on the right hand side of Equation (23) is due to adiabatic variation of gas pressure which has no contribution to the accumulated work as demonstrated in Equation (22). The second term is for the non-adiabatic variation of gas pressure, in which the term $\delta (\rho \epsilon_N)$ is the contribution to gas pressure due to generation of nuclear energy. Generally speaking, it is much less than the last term in the bracket for normal pure p-mode oscillations. We are not going to discuss the details at this point due to limited space. δL_r , δL_c and δL_t are responsible for variations in gas pressure due to radiative and convective (enthalpy and turbulent kinetic) energy transfer. Inserting Equation (23) into Equation (21), the accumulated work (Eq. (21)) can be written as,

$$\begin{aligned} W_{\text{all}} &= \frac{\pi}{2E_K} \int_0^M \left\{ \text{Im} \left[(3\Gamma_3 - 5) x^2 \frac{\delta x}{x} \frac{\delta \bar{\rho}^*}{\bar{\rho}} + \delta \chi_1^1 \frac{d}{d \ln r} \left(\frac{\delta r^*}{r} \right) \right] \right. \\ &\quad \left. - \text{Re} \left[\frac{\Gamma_3 - 1}{4\pi r^2 \bar{\rho} \omega_r} \frac{\delta \bar{\rho}^*}{\bar{\rho}} \frac{d}{dr} (\delta L_r + \delta L_c + \delta L_t) \right] \right\} dw \\ &= W_t + W_{\text{vis}} + W_{P_g r} + W_{P_g c}. \end{aligned} \quad (24)$$

The first set of square brackets under the integral is the contribution to accumulated work due to Reynold's stress, also referred to as the dynamic coupling between convection and oscillations. The

second set of square brackets is that of the radiation and convective (enthalpy and turbulent kinetic) energy transfer.

$$\begin{aligned} W_{P_{gr}} &= \frac{\pi}{2E_K} \int_0^{M_0} \text{Im} \left\{ \frac{\delta\bar{\rho}^*}{\bar{\rho}} \left[\frac{\Gamma_3 - 1}{i\omega\bar{\rho}} \frac{1}{4\pi r^2} \frac{d(\delta L_r)}{dr} \right] \right\} dM_r \\ &= -\frac{\pi}{2\omega E_K} \int_0^{R_0} \text{Re} \left[(\Gamma_3 - 1) \frac{\delta\bar{\rho}^*}{\bar{\rho}} \frac{d(\delta L_r)}{dr} \right] dr, \end{aligned} \quad (25)$$

$$\begin{aligned} W_{P_{gc}} &= \frac{\pi}{2E_K} \int_0^{M_0} \text{Im} \left\{ \frac{\delta\bar{\rho}^*}{\bar{\rho}} \left[\frac{\Gamma_3 - 1}{i\omega\bar{\rho}} \frac{1}{4\pi r^2} \frac{d(\delta L_c + \delta L_t)}{dr} \right] \right\} dM_r \\ &= -\frac{\pi}{2\omega E_K} \int_0^{R_0} \text{Re} \left[(\Gamma_3 - 1) \frac{\delta\bar{\rho}^*}{\bar{\rho}} \frac{d(\delta L_c + \delta L_t)}{dr} \right] dr. \end{aligned} \quad (26)$$

Equations (25) and (26) are the precise formulae for the accumulated work done by radiative and convective energy transfer respectively, in which δL_r and δL_c can be written as,

$$\frac{\delta L_r}{L_r} = \frac{d}{d \ln T} \left(\frac{\delta \bar{T}}{\bar{T}} \right) + (4 - K_T) \frac{\delta \bar{T}}{\bar{T}} - K_P \frac{\delta \bar{P}}{\bar{P}} + 4 \frac{\delta r}{r}, \quad (27)$$

$$\frac{\delta L_c}{L_c} = (A + C_{P,P}) \frac{\delta \bar{P}}{\bar{P}} + (1 - B + C_{P,T}) \frac{\delta \bar{T}}{\bar{T}} + \frac{\delta V}{V} + 2 \frac{\delta r}{r}, \quad (28)$$

where $V = \overline{u_r T'} / \bar{T}$ is the turbulent velocity-temperature correlation, $A = (\partial \ln \rho / \partial \ln P)_T$ and $B = -(\partial \ln \rho / \partial \ln T)_\rho$ are respectively the compression coefficient and thermal expansion coefficient of gas, K and C_P are the radiative opacity of gas and specific heat at constant pressure respectively,

$$K_P = (\partial \ln K / \partial \ln P)_T,$$

$$K_T = (\partial \ln K / \partial \ln T)_P,$$

$$C_{P,P} = (\partial \ln C_P / \partial \ln P)_T$$

and

$$C_{P,T} = (\partial \ln C_P / \partial \ln T)_P$$

are the corresponding partial derivatives with respect to P and T . Considering that oscillations in stellar interiors are normally very close to being adiabatic, we can use the following adiabatic relations when calculating the accumulated work in Equations (25) and (26),

$$(\Gamma_3 - 1) \frac{\delta\bar{\rho}^*}{\bar{\rho}} \approx \frac{\delta\bar{T}^*}{\bar{T}}, \quad \frac{\delta\bar{P}}{\bar{P}} \approx \frac{\delta\bar{T}}{\bar{T}} / \nabla_{ad}. \quad (29)$$

Inserting Equations (27)–(29) into Equations (25) and (26), the following approximate expressions for the accumulated work can be derived,

$$\begin{aligned} W_{P_{gr}} &\approx \frac{\pi}{2\omega_r E_K} \int_0^{R_0} \text{Re} \left\{ L_r \frac{\delta\bar{T}^*}{\bar{T}} \right. \\ &\quad \times \frac{d}{dr} \left[(K_T + K_P / \nabla_{ad} - 4) \frac{\delta\bar{T}}{\bar{T}} - \frac{d}{d \ln T} \left(\frac{\delta\bar{T}}{\bar{T}} \right) - 4 \frac{\delta r}{r} \right] \\ &\quad \left. + \frac{dL_r}{dr} \frac{\delta\bar{T}^*}{\bar{T}} \left[(K_T + K_P / \nabla_{ad} - 4) \frac{\delta\bar{T}}{\bar{T}} - \frac{d}{d \ln T} \left(\frac{\delta\bar{T}}{\bar{T}} \right) - 4 \frac{\delta r}{r} \right] \right\} dr, \end{aligned} \quad (30)$$

$$\begin{aligned}
W_{P_{gc}} \approx & -\frac{\pi}{2\omega_r E_K} \int_0^{R_0} \operatorname{Re} \left\{ L_c \frac{\delta \bar{T}^*}{\bar{T}} \right. \\
& \times \frac{d}{dr} \left[\left(1 - B + C_{P,T} + \frac{A + C_{P,P}}{\nabla_{ad}} \right) \frac{\delta \bar{T}}{\bar{T}} + \frac{\delta V}{V} + 2 \frac{\delta r}{r} \right] \\
& \left. + \frac{dL_c}{dr} \frac{\delta \bar{T}^*}{\bar{T}} \left[\left(1 - B + C_{P,T} + \frac{A + C_{P,P}}{\nabla_{ad}} \right) \frac{\delta \bar{T}}{\bar{T}} + \frac{\delta V}{V} + 2 \frac{\delta r}{r} \right] \right\} dr. \quad (31)
\end{aligned}$$

The first term in the outermost braces of Equation (30) is nothing but the well known radiative κ -mechanism, on which there are very rich discussions in the literature. No more follow up in this work is needed. The second term is what we have called the radiative modulated excitation mechanism (Xiong et al. 1997). Although also being linked to radiative opacity, it is an excitation mechanism for stellar oscillations that is completely different from the radiative κ -mechanism, and it only exists in the radiative zone where there is a gradient in the flux. During the course of stellar oscillations, such a static variation in radiative flux can be modulated by oscillatory motion, and causes transformation between radiative energy and oscillatory kinetic energy. The underlying driving mechanism is somewhat similar to blowing a gentle laminar wind onto a piece of paper, and making the paper vibrate. That is why we call it the radiation modulated excitation mechanism. For the sake of clarity, we will ignore the last two, relatively small, terms $(\frac{d}{d \ln T} (\frac{\delta \bar{T}}{\bar{T}}))$ and $4 \frac{\delta r}{r}$ in the brackets, and we can deduce from Equation (30) that, when

$$(K_T + K_P / \nabla_{ad} - 4) \frac{dL_r}{dr} > 0, \quad (32)$$

this process acts as an excitation, otherwise it is a damping mechanism. In the zone that has a gradient in radiative flux at the top of a convective zone, $K_T + K_P / \nabla_{ad} - 4 > 0$, $dL_r / dr > 0$ and Equation (32) holds, but in the bottom of the radiative zone where there is a gradient in flux, in a deep enough convective zone, one has $K_T + K_P / \nabla_{ad} - 4 < 0$ and $dL_r / dr < 0$, and Equation (32) holds as well. Therefore, the radiative modulated excitation mechanism behaves as an excitation in both radiative zones that have a gradient in flux at the top and bottom of a convective zone. This is exactly the reason why all stars located to the right of the instability strip are unstable, and no red edge of the instability strip can be defined when ignoring the coupling between convection and oscillations.

Figure 8 shows the variation in the accumulated work of the fundamental mode as a function of depth, for a low temperature star located to the red side of the instability strip. The coupling between convection and oscillations is not taken into account here. It is clearly demonstrated in this plot that the major excitation comes from the radiative modulation excitation at the top and bottom of the convective zone. Therefore, we can understand why the cool stars in the right hand side of the HR diagram are pulsationally unstable and no red edge of the instability strip can be found when the convection coupling is ignored.

4.3 Thermodynamic Coupling between Convection and Oscillations

Equation (31) is the component of the accumulated work that comes from transfer of convective energy, which represents the thermodynamic coupling between convection and oscillations. Convection absolutely dominates the energy transfer inside the convective zone (far from both boundaries) for stars having extended convective envelopes, so that we have $L_r \ll L_c$, $L_c \approx L$ and $dL_c / dr \approx 0$. The first term under the integral in Equation (31) is much larger than the second term. Due to the inertia of convective motion, the variations of $\delta V / V$ lag slightly behind those of $\delta T / T$, therefore $W_{P_{gc}} < 0$, i.e. the thermodynamic coupling between convection and oscillations works as a damping mechanism within the deep interior of the convective zone. Furthermore, Equation (31) demonstrates that

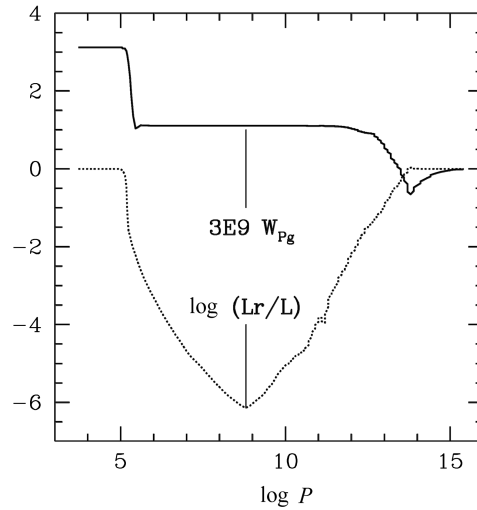


Fig. 8 The accumulated work W_{Pg} (solid line) versus the depth for a low-luminosity red giant star with $M = 1.0 M_{\odot}$, $\log L/L_{\odot} = 0.0830$ and $\log T_e = 3.7523$. The fractional radiation flux (dotted line) is also drawn. The coupling between convection and oscillations is not taken into account here. The two rising parts on the curve at the bottom and top of the convective zone are due to radiative modulation excitation.

W_{Pg} is inversely proportional to the oscillation frequency ω . This means that the damping of thermodynamic coupling between convection and oscillations is stronger for low order modes, therefore it is the major factor for stabilizing oscillations of the low-order modes in low temperature stars.

In the radiative zones that have a gradient in flux at the upper and lower boundaries of the convective layer, the second term of the integral in Equation (31) becomes substantial and cannot be ignored. We refer to this factor as convective modulation excitation, which is distinct from radiative modulated excitation. At the bottom of the convective zone, it behaves as a damping, whereas in the upper boundary it becomes an excitation.

4.4 Dynamic Coupling between Convection and Oscillations

In the following, we are going to discuss the dynamical coupling between convection and oscillations, i.e. the contributions of turbulent Reynold's stress which are precisely expressed by the second and third terms under the integral in Equation (21). δx and $\delta\chi_1^1$ can be derived from linearizing Equations (16) and (17). Equations (16) and (17) both contain a differential term, therefore accurate solutions for δx and $\delta\chi_1^1$ can only be made through numerical integrations for the linear equations describing a non-adiabatic oscillation. The last terms on the left hand side of Equations (16) and (17) come from the third order correlations representing non-local convection transport. Specifically, the term $\bar{\rho} r^2 x l \frac{\partial x^2}{\partial r}$ in Equation (16) is the turbulent kinetic energy flux, which is small compared with other terms in the deep interior of the convective zone far from the boundaries. For simplicity, we will ignore all the third order terms in Equations (16) and (17) for the moment. Linearizing these two equations, we produce the explicit approximate solutions for δx and $\delta\chi_1^1$,

$$\delta x^2 \approx \frac{2}{3} \frac{1}{1 + i\omega\tau_{c1}} \left\{ i\omega\tau_{c1} \left[x^2 \frac{\delta\bar{\rho}}{\bar{\rho}} - \chi_1^1 \frac{d}{d \ln r} \left(\frac{\delta r}{r} \right) \right] \right\}$$

$$+ \frac{GM_r BV \tau_{c1}}{r^2} \left[\frac{\delta V}{V} - \left(2 + \frac{r^3 \omega^2}{GM_r} \right) \frac{\delta r}{r} \right] \Bigg\}, \quad (33)$$

$$\delta \chi_1^1 \approx \frac{4}{3} \frac{1}{1 + i\omega \tau_{c2}} \left\{ -i\omega \tau_{c2} \left[(x^2 + \chi_1^1) \frac{d}{d \ln r} \left(\frac{\delta r}{r} \right) + \frac{3}{2} \chi_1^1 \frac{\delta r}{r} \right] \right. \\ \left. + \frac{GM_r BV \tau_{c2}}{r^2} \left[\frac{\delta V}{V} - \left(2 + \frac{r^3 \omega^2}{gM_r} \right) \frac{\delta r}{r} \right] \right\}. \quad (34)$$

The second and third terms under the integral in Equation (21) are respectively the isotropic and anisotropic components of the turbulent Reynold's stress. The first set of square brackets on the right hand side of Equations (33) and (34) represents the exchange of energy between turbulence and oscillation motions resulting from shear and deformation of the fluid, therefore it reflects turbulent viscosity in the accumulated work; the second square brackets represent the gain of turbulent energy induced by buoyant force. It represents the transformation between thermal energy and kinetic energy of turbulence, thus it acts as the component of turbulent pressure in the accumulated work. Putting Equations (33) and (34) into Equation (21), and after some manipulations, the integrations of the second and third terms can be approximated as the following form,

$$W_{Pt} \approx \frac{2}{3} \frac{\pi}{E_K} \int_0^{M_0} \text{Re} \left\{ \left[\frac{5 - 3\Gamma_3}{4} \frac{\omega \tau_{c1}^2}{1 + \omega^2 \tau_{c1}^2} \frac{\delta \bar{\rho}^*}{\bar{\rho}} \right. \right. \\ \left. \left. - \frac{\omega \tau_{c2}^2}{1 + \omega^2 \tau_{c2}^2} \frac{d}{d \ln r} \left(\frac{\delta r^*}{r} \right) \right] \frac{GM_r BV}{r^2} \right. \\ \left. \times \left[\frac{\delta V}{V} - \left(2 + \frac{r^3 \omega^2}{GM_r} \right) \frac{\delta r}{r} \right] \right\} dM_r, \quad (35)$$

$$W_{vis} \approx -\frac{2}{3} \frac{\pi}{E_K} \int_0^{M_0} \text{Re} \left\{ \frac{\omega \tau_{c1}}{1 + \omega^2 \tau_{c1}^2} \left[x^2 \frac{\delta \bar{\rho}}{\bar{\rho}} - \chi_1^1 \frac{d}{d \ln r} \left(\frac{\delta r}{r} \right) \right] \right. \\ \left. \times \frac{5 - 3\Gamma_3}{4} \frac{\delta \bar{\rho}^*}{\bar{\rho}} + \frac{\omega \tau_{c2}}{1 + \omega^2 \tau_{c2}^2} \left[(x^2 + \chi_1^1) \frac{d}{d \ln r} \left(\frac{\delta r}{r} \right) \right. \right. \\ \left. \left. + \frac{3}{2} \chi_1^1 \frac{\delta r}{r} \right] \frac{d}{d \ln r} \left(\frac{\delta r^*}{r} \right) \right\} dM_r, \quad (36)$$

where $\tau_{c1} = \frac{3}{4} \tau_c$, $\tau_{c2} = \frac{3}{4(1+c_3)} \tau_c$.

Equations (35) and (36) express respectively the effects of turbulent pressure and turbulent viscosity on the stability of stellar oscillations. Noticing that $5 - 3\Gamma_3 \geq 0$ and $\delta V/V$ always slightly lags behind the density variations, the following four characteristics can be concluded:

- (1) Generally speaking, $W_{Pt} > 0$, i.e. turbulent pressure is an excitation against oscillations. This is due to the fact that turbulent pressure normally slightly lags behind density variations due to the inertia of turbulent convective motion. Therefore, on the P_t - V ($= 1/\bar{\rho}$) plane, a positive Carnot cycle is formed, so that the kinetic energy of turbulence is converted into that of oscillation.
- (2) Contrary to the turbulent pressure component W_{Pt} , $W_{vis} < 0$. The physical meaning of that is also very clear: viscosity converts the kinetic energy of stellar oscillations into turbulence due to shear motions. Such a process primarily happens in the low wave number range of the turbulent spectrum. Through the cascading process of turbulence, turbulent kinetic energy gradually shifts from low wave numbers to higher ones, and is eventually converted into the thermal energy of gas by molecular viscosity. If there were no convection, the contribution of molecular viscosity to stellar oscillations could be ignored. However, when convection sets in, the viscosity of fluid motion will greatly increase. In fact, Equations (16) and (17) are the expressions for the conservation of turbulent kinetic energy. In those equations, the first terms describe the rate of

variations for turbulent kinetic energy, the second ones represent the transformation between kinetic energy of the average motion and turbulent one; the third terms are the work done by buoyant force, i.e. transformation between thermal energy and turbulent kinetic energy; while the fourth terms are for a turbulent kinetic energy flux representing the non-local convective diffusion process that makes turbulent kinetic energy go from one place to another. The right hand sides of Equations (16) and (17) are turbulent viscous dissipation terms. Therefore, these two equations actually describe the equilibrium of energy between the pulsating, turbulent and thermal motions. Our non-local and time-dependent theory of turbulent convection is developed based on fluid dynamics and turbulence theory. This can describe the dynamic behaviors of turbulent convection more accurately than MLT.

- (3) The maximum unstable modes: Equations (35) and (36) provide a perspective on the dependence of the dynamic coupling between turbulent convection and oscillations on frequency. When $\omega\tau_{c1} = 1$ or $\omega\tau_{c2} = 1$, the two frequency dependent factors in Equations (35) and (36) reach their maximum. The dynamic coupling between convection and oscillations peak under such a condition. Therefore the frequency of the maximum unstable oscillatory mode can be estimated as $\nu_{\max} \approx 1/2\pi\tau_{c1}$. Taking the Sun as a reference, it follows from Equation (12) that

$$\begin{aligned}\nu_{\max} &\approx \frac{M}{M_{\odot}} \left(\frac{R_{\odot}}{R}\right)^2 \frac{T_{\odot}}{T} \frac{x}{x_{\odot}} \nu_{\max, \odot} \\ &= \frac{M}{M_{\odot}} \frac{L_{\odot}}{L} \left(\frac{T_e}{T_{e, \odot}}\right)^3 \frac{x}{x_{\odot}} \nu_{\max, \odot}.\end{aligned}\quad (37)$$

Within the convective zone of low temperature red stars, the radiative flux is much smaller than the convective flux ($F_c \sim \sigma T_e^4$). It can be shown that $F_c \propto \rho x^3$, therefore,

$$\frac{x}{x_{\odot}} \sim \left(\frac{\rho_{\odot} T_e^4}{\rho T_{\odot}^4}\right)^{\frac{1}{3}} = \left(\frac{M}{M_{\odot}}\right)^{-\frac{1}{3}} \left(\frac{L}{L_{\odot}}\right)^{\frac{1}{2}} \left(\frac{T_e}{T_{e, \odot}}\right)^{-\frac{2}{3}}.\quad (38)$$

Inserting Equation (38) into Equation (37), one will have

$$\nu_{\max} \sim \left(\frac{M}{M_{\odot}}\right)^{\frac{2}{3}} \left(\frac{L}{L_{\odot}}\right)^{-\frac{1}{2}} \left(\frac{T_e}{T_{e, \odot}}\right)^{\frac{7}{3}} \nu_{\max, \odot}.\quad (39)$$

The properties of the maximum unstable mode as estimated by Equation (39) are similar to those given by Equation (3). It is then predicted that for higher stellar luminosities and lower effective temperatures, the maximum unstable mode is shifting towards lower frequencies.

- (4) Estimating the width in frequency for unstable oscillation modes: For the frequency of the maximum unstable mode calculated using Equation (37), the factor $\omega\tau_{c1} / (1 + \omega^2\tau_{c1}^2)$ decreases towards both higher and lower frequencies. The width in frequency of the unstable modes can be measured by locating the points where $\omega\tau_{c1} / (1 + \omega^2\tau_{c1}^2)$ decreases by half. It is trivial to prove that the low frequency half power point is at $\nu_1 = (2 - \sqrt{3}) \nu_{\max}$, while the high frequency one is $\nu_2 = (2 + \sqrt{3}) \nu_{\max}$. The frequency width of unstable modes $\Delta\nu = \nu_2 - \nu_1 = 2\sqrt{3}\nu_{\max}$. It can be seen from Equation (39) that both ν_{\max} and $\Delta\nu$ decrease with increasing luminosity and decreasing effective temperature of stars.

Figure 9 illustrates the general frequency characteristic of W_{P_g} , W_{Pt} and W_{vis} . Through the above analysis and discussions, it is straightforward to understand the properties of low temperature oscillators given in Section 3.

- (1) For all faint low-temperature stars located to the right of the instability strip shown in Figure 1(a), the main cause for them to be stable in low order p-modes is the thermodynamic coupling between convection and oscillations. Equation (31) accurately describes the effects of convective energy transport on the stability of pulsation in stars.

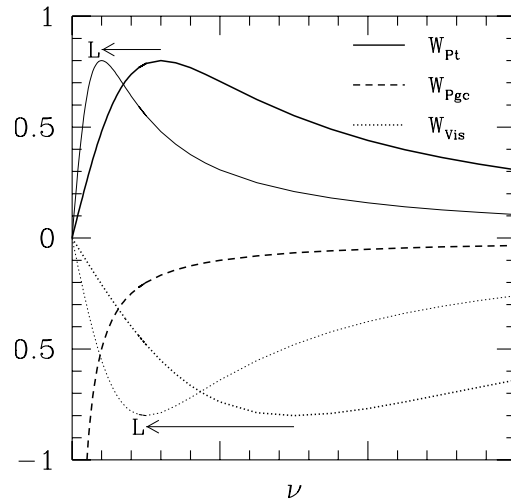


Fig. 9 A sketch showing the frequency dependence of the effects of the convective flux (*dashed line*), turbulent pressure (*solid line*) and turbulent viscosity (*dotted line*) on the pulsational stability of stars. The arrows indicate the directions of movement of the peak for W_{Pt} and W_{vis} when stellar luminosity L increases.

- (2) As shown in Figure 1(b), the intermediate- and high-order p-modes are unstable for all the faint low-temperature stars located to the right hand side of the instability strip. They are excited by turbulent pressure. Figure 9 illustrates W_{Pgc} , W_{Pt} and W_{vis} as functions of frequency. It can be noticed that the maximum excitation due to turbulent pressure is not at the same frequency; instead it changes with the luminosity and effective temperature of stars, as given by Equation (39). For low luminosity red stars, the maximum excitation is at the frequency of the intermediate order modes. This can explain why the Sun, quasi-solar stars and low luminosity red giants are stable in low-order p-modes, but are unstable in intermediate- and high-order p-modes, while possessing a relatively wide frequency width for unstable modes (see Figs. 1 and 2).
- (3) The maximum unstable mode shifts toward low-order modes and, at the same time, the frequency width of unstable modes also decreases with the increase of luminosity and decrease of an effective temperature of the star, as indicated by arrows in Figure 9. This explains why luminous red giants pulsate at only a few low-order modes (see Figs. 1 and 2).

Figure 10(a) and (b) shows accumulated works as functions of depth (in $\log P$) for the radial fundamental mode (a) and 20th overtone mode (b) for the same low luminosity red star as in Figure 8, but with the coupling between convection and oscillations taken into account. The gas pressure (W_{Pg}), turbulent pressure (W_{Pt}) and turbulent viscosity (W_{vis}) components of the accumulated work, as well as the fractional radiative flux L_r/L are plotted. The gas pressure component of accumulated work includes the contributions of both radiative flux and convective flux as shown by Equations (22) and (23). In the deep interior of the convection zone, far from the convective boundary, convection dominates, namely $W_{Pg} \sim W_{Pgc}$. As shown in Figure 10(a) and 10(b), once the coupling between convection and oscillations has been considered, the fundamental mode (and low-order p-modes) becomes stable, but the intermediate- and high-order p-modes are still unstable. Convective energy transfer now works as a damping mechanism, but turbulent pressure acts as an excitation mechanism.

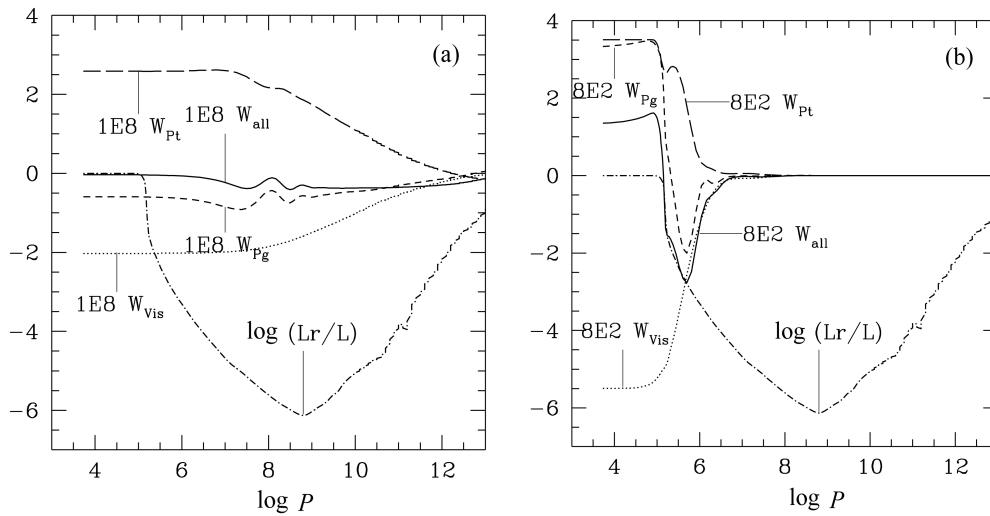


Fig. 10 The accumulated work $W_{\text{all}} = W_{P_g} + W_{P_t} + W_{\text{vis}}$ (solid line) and its gas pressure- (W_{P_g} , dashed line), turbulent pressure- (W_{P_t} , long dashed line) and turbulent viscosity- (W_{vis} , dotted line) components versus the depth for the same low-luminosity red giant star as in Fig. 8. The fractional radiation flux (dashed-dotted line) is also shown. The panel (a) the fundamental mode, the panel (b) p20-mode. The sharp increase of W_{P_g} is due to radiative and convective modulated excitation.

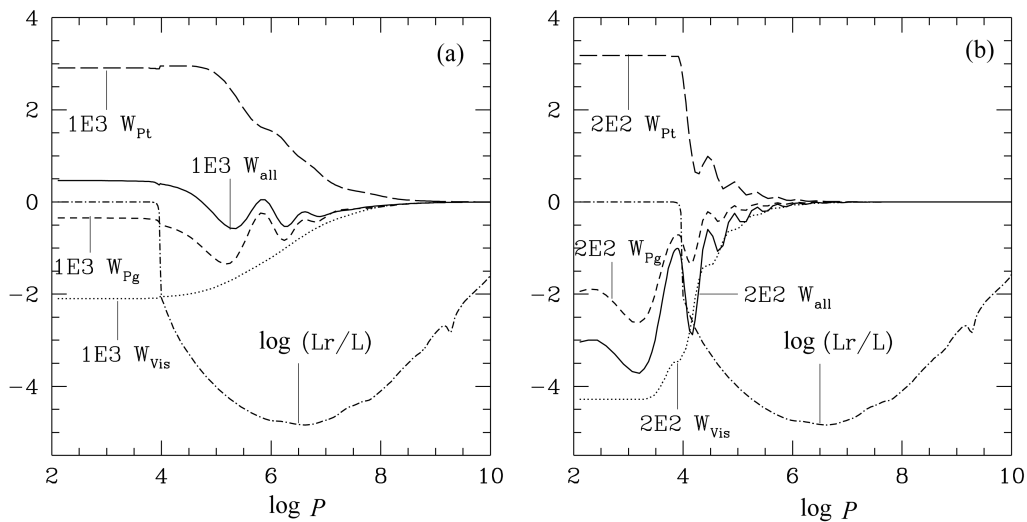


Fig. 11 The same as Fig. 10, but for a luminous red giant star with $M = 1.0 M_{\odot}$, $\log L/L_{\odot} = 2.1905$ and $\log T_e = 3.5855$.

Figure 11(a) and (b) depicts the accumulated works as functions of depth of the fundamental and 20th overtone mode for a luminous red giant. In contrast to the behaviors in Figure 10(a) and (b), the fundamental mode is now unstable, but the 20th overtone mode becomes stable. Turbulent thermal convection and turbulent viscosity are the major damping mechanisms in this case, and turbulent pressure is always an excitation mechanism for oscillations.

The discussions on the accumulated work, including Equations (15)–(36), are all concentrated on radial oscillations of stars. For non-radial oscillation in stars, modifications to the above formalisms have to be applied (Xiong & Deng 2010). However, the effects of convective flux, turbulent pressure and turbulent viscosity on instabilities in stellar oscillation, together with the conclusions drawn about the frequency dependence are all also qualitatively correct for non-radial oscillations. In fact, stellar radial oscillations can be regarded as particular cases of non-radial oscillations when $l = 0$. It follows from Figures 3–7 that the main properties of radial and non-radial oscillations are very similar; amplitude growth rates of oscillations only depend on oscillation frequency ν , and have nothing to do with the degree l of spherical harmonics. This is true at least for intermediate- and low-degree oscillations of $l \leq 25$ in stars (Xiong & Deng 2010).

5 DISCUSSION

This work is one in a series of papers on turbulent convection and pulsation stability. In this work, we present the numerical results of the radial and low-degree ($l = 1 - 4$) non-radial, non-adiabatic oscillations from zero age main sequence to AGB stars with stellar masses ranging from 0.6 to $3.0 M_{\odot}$. The results show that the low-luminosity, low-temperature stars behave as solar-like oscillators, whereas the luminous red giants possess Mira-like oscillation properties.

For low-temperature stars with extended convective envelopes, the coupling between convection and oscillations serves as the major mechanism for excitation and damping. Convection acts on stellar stability through convective energy transfer, turbulent pressure and turbulent viscosity. We have carried out very careful analysis of the effects of the above-mentioned factors on stellar stability, and the results of our studies show that, in the deep interiors of the convective zone far away from the boundaries, thermal convection works as a damping mechanism, and the damping is inversely proportional to oscillation frequency. Thermodynamic coupling between convection and oscillations is the reason for the existence of the red edge of the Cepheid instability strip. On the contrary, turbulent pressure is usually an excitation of oscillations, because of the fact that turbulent pressure P_t always slightly lags behind variations in gas density due to the inertia of convective motions in the course of stellar pulsations.

As a result, a positive Carnot cycle is formed in the P_t – V ($V = 1/\rho$) plane, i.e. turbulent kinetic energy is converted into that of pulsation, yielding an excitation mechanism. Turbulent viscosity tends to convert pulsation kinetic energy into turbulent kinetic energy in the low-wave number regime, and eventually into heat at high wave numbers through cascading processes of turbulence. Therefore turbulent viscosity is always a damping against oscillations. The excitation of turbulent pressure and the damping of turbulent viscosity reach their corresponding maxima respectively at $3\omega\tau_c/4 \sim 1$ and $3\omega\tau_c/4(1 + c_3) \sim 1$ (ω is the circular frequency and $\tau_c = c_1 r^2 P / 0.78 G M_r \rho x$ is the dynamic time scale of convective motions). For lower temperature and higher luminosity, τ_c increases, therefore the most unstable mode in a star is shifted towards lower order. This is the reason why low-luminosity, low-temperature stars usually show solar-like oscillations, but the luminous red giants display Mira-like oscillations.

Our theory of non-local and time-dependent convection is based on the hydrodynamic equations and the theory of turbulence. Compared with the phenomenological mixing-length theories, ours is more physically sound and more accurate in describing the dynamic behaviors of turbulent convection in stars. Our theory can be regarded as a system of dynamic equations of auto- and cross-correlations, which contain two (c_1 and c_2 in the approximation of quasi-isotropic turbulence) or three (plus c_3 describing anisotropy of turbulence) adjustable parameters. c_1 , c_2 and c_3 describe respectively the turbulent dissipation, the turbulent diffusion and the anisotropy of turbulent convection. Explaining a problem by tuning a parameter in a theory is a usual practice in astrophysical research. In our case, by using the same set of convective parameters (c_1 – c_3) that were calibrated by solar observations, we successfully reproduced a variety of solar and stellar observations, including

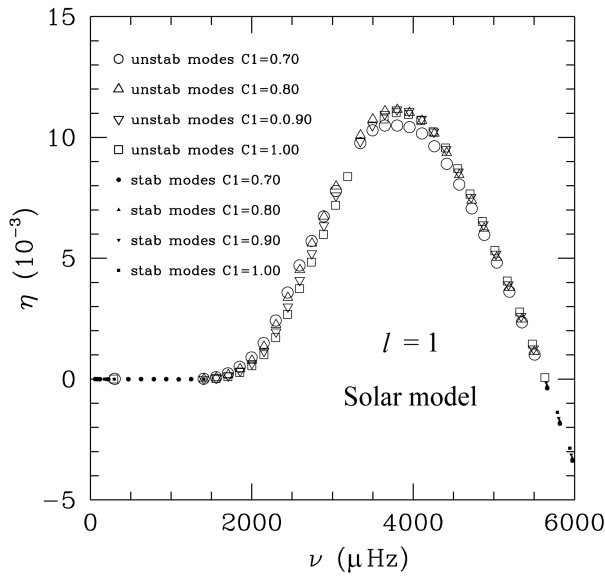


Fig. 12 The amplitude growth rates $\eta = -2\pi\omega_i/\omega_r$ versus frequencies for four solar envelope modes with different connection parameters, $c_1 = 0.7$ (circles), 0.8 (triangles), 0.9 (inverse triangles) and 1.0 (squares), where $c_2 = c_1/2$. The small solid symbols and large open symbols are used for the stable and the unstable modes respectively.

the structure of the solar convective zone (Unno et al. 1985; Xiong & Deng 2001b; Zhang et al. 2012), the atmospheric lithium abundances of the Sun and solar-type stars (Xiong & Deng 2009), evolution of massive stars (Xiong 1986), RR Lyrae and the δ Scuti instability strip (Xiong et al. 1998b; Xiong & Deng 2001a), and the general observational properties of oscillations in Mira stars and red giants (Xiong et al. 1998a; Xiong & Deng 2007). All these works served as a demonstration that our theory is rather robust in stellar physics. We would like to emphasize here that the results of non-adiabatic oscillations of stellar models hardly depend on the tuning of the parameters (Xiong et al. 1998b). The results of solar convective envelope models calculated using four sets of parameters, $c_1 = 0.7, 0.8, 0.9, 1.0$, and $c_2 = c_1/2$, are presented in Figure 12, in which the amplitude growth rate as a function of frequency for the non-radial p-mode of $l = 1$ is drawn. It can be made clear from the plot that by changing the parameter by almost a factor of 1.4 times (far larger than the range of its uncertainty), the stability of the p-mode only varies by a small amount. Therefore, we are rather confident to conclude that the main results of the current work are not compromised by any choice of the convective parameters in the theory. Concluding from the work done for very different stellar convection problems, our theory describing stellar convection is robust in handling the dynamic behaviors of stellar convection.

We are certain that the turbulent stochastic excitation is the excitation that is responsible for high-degree/order mode oscillations in the Sun and in low-luminosity, low-temperature stars. Comparing the line width of solar p-modes (Libbrecht 1988; Chaplin et al. 1997) and the amplitude growth rates calculated by us, one can easily see that it is not possible to have observed amplitudes in high frequency modes ($\nu > 4000$ Hz) with the coupling between convection and oscillations alone. However, for the solar p-modes with intermediate frequency ($\sim 1000 \mu\text{Hz} < \nu < 3500 \mu\text{Hz}$), the excitation of the coupling between convection and oscillations is powerful enough to compen-

sate the damping indicated by the line widths in those modes, so that those modes can be excited. Therefore we would argue that five-minute solar oscillations cannot be a result of one single mechanism; instead they are driven by the combination of turbulent stochastic excitation and the “regular” convective coupling. For intermediate- and low-frequency modes, the coupling between convection and oscillations dominates, while in high-frequency modes, turbulent stochastic excitation takes over (Xiong & Deng 2010).

No doubt, the assessment on the excitation mechanism of solar five-minute oscillations discussed above is solely based on a number of theoretical reasonings, and it definitely needs observations to back it up. Using 200 day solar radial velocity data taken by GOLF onboard SOHO, García et al. (2001) discovered a peak at $\nu = 284.67 \mu\text{Hz}$ in the power spectrum with 98% confidence. Later in 2002, Gabriel et al. independently confirmed such an observation using a statistical approach, verifying the signal at 96% confidence. Coincidentally, the theoretical modeling of solar non-radial and non-adiabatic oscillations also shows that the p_1 mode of $l = 1$ is unstable, which has a theoretical oscillation frequency of $\nu \approx 284.1 \mu\text{Hz}$. Meanwhile, all other g- and p-modes having similar frequencies are stable (Xiong & Deng 2012). If the discovery of García et al. and Gabriel et al. were both correct, it can serve as solid support for our theory.

Restricted to solar oscillations, the turbulent stochastic excitation mechanism is more developed and successful compared to our theory, due to its clarity, and can be strongly supported by observations in the following two aspects.

- (1) With a certain choice of convection parameter, the observed line widths of solar p-mode oscillations can be reproduced fairly well (Balmforth 1992; Libbrecht 1988; Chaplin et al. 1997);
- (2) Under some specific assumptions on the spectra of turbulence, the observed amplitude in velocity of solar five-minute oscillations can be approximately reproduced (Libbrecht 1988; Balmforth 1992; Goldreich & Kumar 1988; Samadi et al. 2003; Belkacem et al. 2008).

One of the fundamental ideas of the turbulent stochastic excitation mechanism is that solar oscillations are pulsationally stable, and are damped by convection. Whether solar oscillations are stable or unstable has been a rather disputed theoretical problem that sensitively depends on the treatment of convection (Ulrich & Rhodes 1977; Antia et al. 1982; Antia et al. 1988; Samadi et al. 2002; Balmforth 1992). Suddenly after the measurement of the limited line widths of solar p-mode oscillations, the damped solar five-minute oscillations became an undisputed fact in the community. Is that really completely unchallengeable? Of course, a linear stable mode must have a limited width, but on the other hand, one may conclude differently going backward, i.e. limited width may not necessarily be the result of linear stability. For a straightforward example, a chain of quasi “monochromatic” light waves, with limited length or with its amplitude/phase being modulated, will always be observed as having limited width. This is because in most cases, we cannot observe the true profile of a spectral line. This is not solely due to restrictions on observational techniques; even if observations were perfect, the true line profile still could not be observed due to the limited lifetime of the oscillation mode that puts a limit on the resolution of the spectrum. That is why we say that “observations give a seemingly limited line width.” For classical variables with small amplitudes such as δ Scuti and β Cephei, observations will also show limited line widths. There are no observations that confirm this behavior, simply because no attempts have been made so far. Nevertheless, we can never conclude that the oscillations in all red giants are linearly stable by extrapolating the turbulent stochastic excitation mechanism established in solar studies. In fact, Mira, semi-regular and irregular variables cannot be explained at all using turbulent stochastic excitation; instead it is widely accepted that the coupling between convection and oscillations is their driving mechanism. It is hard to believe that a mechanism having such a major effect happens all of a sudden in luminous red giants. A more logical reasoning will be that such a mechanism already exists in low-luminosity, low-temperature stars, and it becomes stronger with higher luminosity. This is a rather gradual process of change. Although it is not possible to define the exact location in the H-R diagram and the exact frequency

where the transition between these two competing mechanisms happens, the transition point must still exist as nature obeys physical laws. In this sense, the series of work done so far using our theory has provided a unified approach to a number of connected problems, namely the red edge of the Cepheid instability strip, solar-like oscillations in low-luminosity cases, and Mira-like oscillations in luminous red giants. That is not to say that the theory itself is already perfect; instead much more still needs to be done in order to further improve it.

Our non-local, time-dependent theory of convection is a type of statistical theory of correlations, or more precisely, it is composed of a set of dynamic equations of squared turbulent velocity, temperature fluctuations and turbulent velocity-temperature fluctuation correlations related by some statistical average. Such a statistical average is made either at a characteristic length shorter than the wavelength of standing waves and on a spherical surface large enough compared to the characteristic dimension of turbulent elements in space, or shorter than the oscillation period and longer than the characteristic time scale of turbulence in time. As a result, the theory we developed is only suitable for static convection and modes with low-frequency (low-degree and low-order) oscillations. For modes with high frequency oscillations, the wavelength of oscillation and the characteristic scale length of turbulent eddies is compatible; the oscillation period and the characteristic time scale of turbulent elements are also of the same order, and the statistical averaging method embedded in our theory is no longer appropriate, therefore the conclusions will no longer be valid. Therefore, it is problematic to apply in modes with high frequency. For higher and higher frequencies, the stochastic nature of turbulence overwhelms this process. To conclude, our statistical theory of turbulent convection is a good approach for static stellar convection and analysis of low-frequency oscillations, and the turbulent stochastic mechanism should work better for high-frequency (high-order/high-degree) oscillations in stars. Unfortunately, the development of stellar convection theory still has to overcome obstacles, since there is currently no good way to handle problems in both low-frequency and high-frequency domains.

When turbulence is propagating in inhomogeneous media, sound waves may be scattered or refracted by turbulent eddies, causing energy loss and phase shifts. Both damage the coherence of the standing waves (Gough 1980). The shorter the sound wavelength is, the stronger these effects become. In the current work, we completely ignored the effects of scattering and refractions due to turbulence. As a result of such a treatment, damping at high frequency is underestimated for solar and solar-like oscillations. Such a problem has already been shown in the numerical results. For instance, the theoretical prediction is that the most unstable mode falls at $\nu_{\max} \sim 3800 \mu\text{Hz}$ (see Fig. 3), but the observed one is located at $\nu_{\max} \sim 3020 \mu\text{Hz}$.

Acknowledgements The National Natural Science Foundation of China is acknowledged for support (Grant Nos. 11073053 and 10973015). We are grateful to the referee for careful reading of the paper and helpful discussion.

References

- Alexander, D. R., & Ferguson, J. W. 1994, *ApJ*, 437, 879
Antia, H. M., Chitre, S. M., & Narasimha, D. 1982, *Sol. Phys.*, 77, 303
Antia, H. M., Chitre, S. M., & Gough, D. O. 1988, in *IAU Symposium*, 123, *Advances in Helio- and Asteroseismology*, eds. J. Christensen-Dalsgaard, & S. Frandsen (D. Reidel Publ. Co. Dordrecht), 371
Balmforth, N. J. 1992, *MNRAS*, 255, 603
Barban, C., Matthews, J. M., De Ridder, J., et al. 2007, *A&A*, 468, 1033
Bedding, T. R., & Kjeldsen, H. 2007, *Communications in Asteroseismology*, 150, 106
Belkacem, K., Samadi, R., Goupil, M.-J., & Dupret, M.-A. 2008, *A&A*, 478, 163
Böhm-Vitense, E. 1958, *ZAp*, 46, 108
Bouchy, F., & Carrier, F. 2002, *A&A*, 390, 205

- Brown, T. M., Gilliland, R. L., Noyes, R. W., & Ramsey, L. W. 1991, *ApJ*, 368, 599
- Buzasi, D., Catanzarite, J., Laher, R., et al. 2000, *ApJ*, 532, L133
- Chaplin, W. J., Elsworth, Y., Isaak, G. R., et al. 1997, *MNRAS*, 288, 623
- Chaplin, W. J., Kjeldsen, H., Bedding, T. R., et al. 2011a, *ApJ*, 732, 54
- Chaplin, W. J., Kjeldsen, H., Christensen-Dalsgaard, J., et al. 2011b, *Science*, 332, 213
- Daeppen, W., Mihalas, D., Hummer, D. G., & Mihalas, B. W. 1988, *ApJ*, 332, 261
- De Ridder, J., Barban, C., Baudin, F., et al. 2009, *Nature*, 459, 398
- Deng, L., Xiong, D. R., & Chan, K. L. 2006, *ApJ*, 643, 426
- Dupret, M. A., Barban, C., Goupil, M.-J., et al. 2006, in *Proceedings of SOHO 18/GONG 2006/HELAS I, Beyond the spherical Sun (ESA Special Publication)*, 624
- Dziembowski, W. A., Gough, D. O., Houdek, G., & Sienkiewicz, R. 2001, *MNRAS*, 328, 601
- Frandsen, S., Carrier, F., Aerts, C., et al. 2002, *A&A*, 394, L5
- Gabriel, M. 1988, in *IAU Symposium*, 123, *Advances in Helio- and Asteroseismology*, eds. J. Christensen-Dalsgaard, & S. Frandsen (D. Reidel Publ. Co., Dordrecht), 375
- Gabriel, A. H., Baudin, F., Boumier, P., et al. 2002, *A&A*, 390, 1119
- García, R. A., Régulo, C., Turck-Chièze, S., et al. 2001, *Sol. Phys.*, 200, 361
- Goldreich, P., & Keeley, D. A. 1977a, *ApJ*, 211, 934
- Goldreich, P., & Keeley, D. A. 1977b, *ApJ*, 212, 243
- Goldreich, P., & Kumar, P. 1988, *ApJ*, 326, 462
- Goldreich, P., Murray, N., & Kumar, P. 1994, *ApJ*, 424, 466
- Gough, D. O. 1977, *ApJ*, 214, 196
- Gough, D. 1980, in *Nonradial and Nonlinear Stellar Pulsation, Lecture Notes in Physics*, eds. H. A. Hill, & W. A. Dziembowski (Berlin: Springer Verlag), 125, 273
- Grigahcène, A., Dupret, M.-A., Gabriel, M., Garrido, R., & Scuflaire, R. 2005, *A&A*, 434, 1055
- Guenther, D. B., Kallinger, T., Reegen, P., et al. 2005, *ApJ*, 635, 547
- Hekker, S., Elsworth, Y., De Ridder, J., et al. 2011, *A&A*, 525, A131
- Houdek, G. 2008, *Communications in Asteroseismology*, 157, 137
- Huber, D., Bedding, T. R., Stello, D., et al. 2011, *ApJ*, 743, 143
- Hummer, D. G., & Mihalas, D. 1988, *ApJ*, 331, 794
- Kumar, P., Franklin, J., & Goldreich, P. 1988, *ApJ*, 328, 879
- Kumar, P., & Goldreich, P. 1989, *ApJ*, 342, 558
- Leighton, R. B., Noyes, R. W., & Simon, G. W. 1962, *ApJ*, 135, 474
- Libbrecht, K. G. 1988, *ApJ*, 334, 510
- Libbrecht, K. G., & Woodard, M. F. 1991, *Science*, 253, 152
- Libbrecht, K. G., & Zirin, H. 1986, *ApJ*, 308, 413
- Rogers, F. J., & Iglesias, C. A. 1992, *ApJS*, 79, 507
- Samadi, R., & Goupil, M.-J. 2001, *A&A*, 370, 136
- Samadi, R., Houdek, G., Goupil, M.-J., Lebreton, Y., & Baglin, A. 2002, in *Stellar Structure and Habitable Planet Finding (ESA Special Publication)*, eds. B. Battrick, F. Favata, I. W. Roxburgh, & D. Galadi, 485, 87
- Samadi, R., Nordlund, Å., Stein, R. F., Goupil, M. J., & Roxburgh, I. 2003, *A&A*, 403, 303
- Samadi, R., Belkacem, K., Goupil, M.-J., Ludwig, H.-G., & Dupret, M.-A. 2008, *Communications in Asteroseismology*, 157, 130
- Spiegel, E. A. 1963, *ApJ*, 138, 216
- Stellingwerf, R. F. 1982, *ApJ*, 262, 330
- Stello, D., Bruntt, H., Kjeldsen, H., et al. 2007, *MNRAS*, 377, 584
- Ulrich, R. K. 1970a, *ApJ*, 162, 993
- Ulrich, R. K. 1970b, *Ap&SS*, 7, 183
- Ulrich, R. K., & Rhodes, E. J., Jr. 1977, *ApJ*, 218, 521

- Unno, W. 1967, PASJ, 19, 140
Unno, W., Kondo, M.-A., & Xiong, D.-R. 1985, PASJ, 37, 235
Xiong, D. 1981, Scientia Sinica, 24, 1406
Xiong, D. 1985, A&A, 150, 133
Xiong, D.-R. 1986, A&A, 167, 239
Xiong, D.-R. 1989, A&A, 209, 126
Xiong, D. R., Cheng, Q. L., & Deng, L. 1997, ApJS, 108, 529
Xiong, D. R., Deng, L., & Cheng, Q. L. 1998a, ApJ, 499, 355
Xiong, D. R., Cheng, Q. L., & Deng, L. 1998b, ApJ, 500, 449
Xiong, D. R., & Deng, L. 2001a, MNRAS, 324, 243
Xiong, D. R., & Deng, L. 2001b, MNRAS, 327, 1137
Xiong, D. R., & Deng, L. 2007, MNRAS, 378, 1270
Xiong, D. R., & Deng, L. 2009, MNRAS, 395, 2013
Xiong, D. R., & Deng, L. 2010, MNRAS, 405, 2759
Xiong, D. R., & Deng, L. 2012, Acta Astron. Sinica, 54, 20
Zhang, C., Deng, L., Xiong, D., & Christensen-Dalsgaard, J. 2012, ApJ, 759, L14